Thermal-optical analysis of snow samples – challenges and perspectives introduced via the occurrence of mineral dust

Daniela Kau[1], Marion Greilinger[2], Bernadette Kirchsteiger[1], Aron Göndör[1], Christopher Herzig[1], Andreas Limbeck[1], Elisabeth Eitenberger[1], and Anne Kasper-Giebl[1]

[1]Institute of Technologies and Analytics, TU Wien, Vienna, 1060, Austria
[2]Zentralanstalt für Meteorologie und Geodynamik (ZAMG), Vienna, 1190, Austria

Correspondence to: Daniela Kau (daniela.kau@tuwien.ac.at)

Abstract. The determination of mineral dust and elemental carbon in snow samples is of great interest, as both compounds are known as light absorbing snow impurities. Different analytical methods have to be used to quantify both compounds. Still, the occurrence of mineral dust, which contains hematite, leads to a bias in the quantification of elemental carbon via thermal-optical analysis. Here we present an approach which utilizes this interference to determine the concentration of hematite via thermal-optical analysis using a Lab OC/EC Aerosol Analyzer (Sunset Laboratory Inc.) and the EUSAAR2 protocol. Therefore, the temperature dependency of the transmittance signal determined during the calibration phase, i.e. when all carbonaceous compounds are already removed, is evaluated. Converting the transmittance signal into an attenuation, a linear relationship between this attenuation and the hematite loading is obtained for loadings ranging from 10 to 100 µgFe cm⁻². Furthermore, the approach allows to identify samples which need to be re-evaluated, as the analysis of elemental carbon is biased by mineral dust. We discuss the successful application of the method, designed for snow samples, to ambient air samples containing mineral dust, and the limitations of the method when other iron compounds besides hematite are present.

1 Introduction

Black carbon (BC) and mineral dust (MD) have been identified and evaluated as prominent light absorbing snow impurities (LASI) (Warren and Wiscombe, 1980; Svensson et al., 2018; Kaspari et al., 2014; Doherty et al., 2016; Tuzet et al., 2017). Deposition of these compounds leads to a reduction of the surface albedo, influencing thawing and geochemical processes, accelerating snow and ice melt and triggering albedo feedback (Ramanathan and Carmichael, 2008, Tuzet et al., 2020).

The presence of MD in snow can be determined via gravimetric measurements (e.g. Kuchiki et al., 2015), particle counting methods (e.g. Di Mauro et al., 2015) or is calculated based on the concentrations of iron, calcium, aluminum, silicon and titanium (Li et al., 2017).

Quantification of BC concentrations in snow and ice has been done via several methods, which are addressing either BC or elemental carbon (EC). Thermal-optical analysis (Chow et al., 1993; Birch and Cary, 1996), optical methods determining the spectral absorption of total particulate matter sampled on a filter (Grenfell et al., 2011) and laser-induced incandescence (Schwarz et al., 2006) are commonly applied. Regarding the differentiation between BC and EC we refer to the thorough discussion in Petzold et al. (2013). Reviews and comparisons of advantages and disadvantages of the respective methods can be found in literature (Lim et al., 2014; Qian et al., 2015; Kang et al., 2020). Within this work we will focus on thermal-optical analysis (TOA), which allows to differentiate between organic carbon (OC) and EC and represents the reference method for analysis of OC and EC in particulate matter samples (DIN EN 16909:2017). The filter is heated in an inert (helium) and subsequently in an oxidizing (helium/oxygen) atmosphere, while the evolving carbon is converted to methane and determined with a flame ionization detector. To account for pyrolysis and to separate OC and EC precisely, the transmittance or reflectance of the filter is monitored. The time when the transmittance (or reflectance) reaches its initial value determines the split point to differentiate between OC and EC. Several temperature protocols were introduced to optimize the method (e.g. Cavalli et al., 2010; Chow et al., 2007). Liquid samples can be analyzed after filtration, when water insoluble OC (WinsOC) and EC are

40 retained on a quartz fiber filter. Previous works address uncertainties related to the filtration process like an undercatch during the filtration, uneven filter loadings or the loss of EC within vessels used for melting and filtration (Forsström et al., 2013; Torres et al., 2014; Lim et al., 2014; Kuchiki et al., 2015; Meinander et al., 2020).

Uncertainties related to TOA itself apply to both, the analyses of filter residues of liquid samples and the analyses of particulate matter samples, even though there might be some basic differences between the two types of samples, such as a differing

45 particle size distribution or a slightly modified chemical composition. As we focus on the analytical procedure of TOA, we will avoid the term WinsOC throughout the manuscript and stick to OC. This highlights that the differentiation between WinsOC filtrated from liquid samples and OC in particulate matter is not the main point and the concept can be applied to the analysis of both sample types. The OC/EC split and thus the quantification of EC is influenced by the overall chemical composition. When elevated loadings of MD are present the influence of carbonates (Li et al., 2017; Karanasiou et al., 2011)

50 and metal oxides (Bladt et al., 2012; Bladt et al., 2014) is important, as MD is rich in those compounds (e.g. Kandler et al., 2007). The effect of iron oxides, namely hematite, is of special importance. Causing the reddish color of the dust, hematite makes MD a prominent component of LASI, and affects TOA. Wang et al. (2012) identified an extra decrease in optical reflectance during the 250°C heating stage due to hematite and suggested to adjust the method accordingly. Gul et al. (2018) suggested to enhance these adjustments even further, defining the reference value for the OC/EC split at 550°C for filters with

55 higher MD loads.

In this work we investigate the use of TOA for the analysis of LASI in snow and particulate matter samples collected in a high alpine environment. To exceed the method's limit of detection, filtrating a rather large amount of liquid snow or ice is desirable. By doing so the enrichment of MD containing hematite might lead to the interference mentioned above. The main interest of our work is not the definition of the ideal reference to set an accurate OC/EC split point, but the investigation of the temperature

60 dependence of the light attenuation caused by hematite. This led us to a new approach to approximate hematite concentrations via TOA. Therefore, we evaluate the transmittance signal during the calibration phase, i.e. when carbonaceous compounds are no longer present. The method is tested extensively for snow samples and evaluated briefly for particulate matter samples.

2 Collection of samples and sample preparation

2.1 Snow samples

65 Surface snow samples were collected near the global GAW (Global Atmosphere Watch) station Sonnblick Observatory, situated at 3106 m a.s.l., in the Austrian Alps. MD deposited on Mount Sonnblick often derives from long range transport of dust from desert regions (Greilinger et al., 2018). For sampling, the uppermost centimeters of snow were collected directly in Whirl-Pak™ bags (Nasco™). For this purpose, the bag was opened and the opening, which is reinforced by a wire handle, was used as a shovel to scoop in the top snow layer. Samples with and without a visible influence of MD were collected during

70 multiple visits at the station between 2018 to 2020 and were kept frozen until further processing. In the laboratory, samples (approximately 600 g each) were melted gently in a glass beaker using a microwave (600 W). Aliquots of the liquid samples were filtrated onto precleaned (24 h at 600°C, cooling in a desiccator above distilled water) quartz fiber filters (Pallflex® Tissuquartz™; loaded area was circular with a diameter 16 mm of which one half was used for analysis) applying a slight vacuum. After filtration, filters were dried overnight in a desiccator above silica gel to allow further analysis.

75 Blank filters were prepared in a similar way, filtrating ultrapure water instead of the liquid snow sample.

2.2 PM$_{10}$ samples

PM$_{10}$ was sampled onto quartz fiber filters (Pallflex® Tissuquartz™) in the same high alpine environment as the snow samples using a high volume sampler (DIGITEL Elektronik AG, Switzerland; sampling duration: 1 week) and in tunnels with railway traffic using a low volume sampler SEQ47/50 (Sven Leckel Ingenieurbüro GmbH, Germany; sampling duration: 4 h). No

80   precleaning step of the filters was performed before sampling. Rectangular aliquots with an area of 1.5 cm² were used for analysis.

2.3 Reference samples containing hematite

Hematite (Fe_2O_3) has been identified as the light absorbing compound in MD before (e.g. Alfaro et al., 2004; Wang et al., 2012) and was used as a reference substance. Fe_2O_3 was suspended in ultrapure water (8.75 mg in 1 l flask) in an ultrasonic

85   bath. Quartz fiber filters were loaded with different amounts of the suspension to cover the range of the Fe loadings found on filters loaded with snow samples containing MD (roughly 12 to 314 µgFe cm^{-2}).

3 Instrumentation

3.1 Thermal-optical analysis

Thermal-optical analysis (TOA) was conducted using the Lab OC-EC Aerosol Analyzer (Sunset Laboratory Inc., USA) and

90   the EUSAAR2 protocol (Cavalli et al., 2010). The instrument logs the transmittance and reflectance of the sample at a wavelength of 660 nm during the measurement. For the measurement, the program OCEC834 and for the evaluation of the raw data the program Calc415 (both Sunset Laboratory Inc., USA) were used. Further processing of the transmittance data was conducted with an external program (Microsoft Excel, Microsoft Corporation, USA).

3.2 Inductively coupled plasma-optical emission spectroscopy and -mass spectrometry

95   After TOA, the filter aliquots of the snow samples, Fe_2O_3 samples and high alpine PM_{10} samples were digested using a microwave system (Multiwave 5000, Anton Paar, Austria) and METHOD 3052 (US EPA, 1996; HNO_3:HCl:HF 6:2:1) and were analyzed for Fe via inductively coupled plasma-optical emission spectroscopy (ICP-OES; iCAP 6500 ICP-OES spectrometer, Thermo Scientific, USA). Filter aliquots of the particulate matter samples collected within the railway tunnel were digested using a microwave system (Multiwave 3000, Anton Paar, Austria/Start1500, MLS GmbH, Germany; aqua regia,

100   maximum temperature: 220°C) and Fe was quantified via inductively coupled plasma-mass spectrometry (ICP-MS; iCap Q System instrument, Thermo Scientific, USA).

3.3 X-ray powder diffraction

X-ray powder diffraction (PXRD) experiments in Bragg Brentano geometry were carried out using an Empyrean diffractometer (Malvern PANalaytical B.V., Netherlands; scattering angle range of 5° < 2θ < 135°). A focussing mirror was

105   used to provide Cu K$_{\alpha1,2}$- radiation for the experiment. The beam divergency was defined by using a 1/4° fixed vertical entrance slit followed up by a 0.04 rad horizontal Soller slit and a 0.04 rad horizontal Soller slit on the secondary side in front of an open line detector (GaliPix detector). The detector to sample distance for this instrument was fixed to 240 mm.

The PXRD diagrams were evaluated using the Malvern PANalytical program suite HighScorePlus v4.6a (Degen et al., 2014). A background correction and a K$_{\alpha2}$ strip were performed. Crystallographic phases were assigned based on the ICDD-PDF4+

110   database (Kabekkodu et al., 2002).

3.4 Scanning electron microscopy

Quartz fiber filters loaded with snow samples and the reference substance Fe_2O_3 were analyzed by scanning electron microscopy (SEM). A FEI Quanta 200 (Thermo Fisher Scientific, USA) instrument equipped with an Octane Pro EDS System (EDAX, USA) was used.

4 Results and Discussion

4.1 Transmittance of filters loaded with snow samples during TOA

During TOA of snow samples, the transmittance of the filters changes due to pyrolysis and removal processes of carbonaceous compounds, resulting in a clean filter after the analysis is completed. However, if MD is present, the filters remain colored and the transmittance stays lower than for a clean filter, even after the complete removal of carbon. Thus, the transmittance, and respective changes of this value observed throughout TOA, can either be due to the carbon load or MD. The influence of the various compounds becomes visible when the same filter is analyzed repeatedly, as illustrated in Fig. 1. The change in transmittance of a filter loaded with a snow sample without visible MD contamination during TOA is given in Fig. 1a, while Figure 1b shows the results obtained for a snow sample containing MD. For both samples, multiple measurements (three to five reruns) of the same filter were conducted to separate the change in transmittance deriving from carbonaceous compounds and from MD, which is left on the filter as a residue after the first analysis run. The course of the transmittance signal within the first run, when carbonaceous compounds are still present, is given as a black line. The average course of transmittance of the reruns is shown as a grey line, whereas the standard deviation of the reruns is plotted as a grey area. The reported temperature (red line) is the temperature inside the sample oven. The vertical lines denote the switch from an inert (He) to an oxidizing atmosphere (He/O_2) and the start of the calibration phase (Cal). Before introducing oxygen and starting the second temperature profile, the temperature is reduced temporarily. At the end, the thermogram includes a cooling phase. At that time, calibration is performed. The part of this cooling phase, which will be used for further evaluations, is highlighted in orange. The Fe loading on the filter loaded with MD was 30 µgFe cm^{-2}, while it was below 2.5 µgFe cm^{-2} for the sample without visible MD contamination. The total carbon loads on the filters were 66 µgC cm^{-2} (sample containing MD) and 28.5 µgC cm^{-2} (sample without MD), but for better clarity, the FID signal is not shown in any panel of Figure 1.

Both samples, with and without MD, show pronounced changes of the transmittance signal during the first analysis represented by the black line. Changes are more pronounced in Figure 1b, which can be expected due to the higher total carbon load. For the sample without MD (Figure 1a), the split point could be set automatically and was reached during the EC3 phase, i.e. the third temperature step during the oxidizing phase. For the sample containing MD (Figure 1b), the initial transmittance was never reached, and thus no EC would be determined. Applying the approach described by Wang et al. (2012), i.e. using the transmittance at 250°C as a reference if MD is present, still no split point can be determined before the cooling phase starts. Using the approach of Gul et al. (2018) and taking the transmittance at 550°C as a reference, an identification of EC becomes possible.

During the reruns (grey line) only minor changes in the transmittance signal are determined for the sample without MD, which is in good agreement with the recordings obtained for the blank filter (Fig 1c). The sample containing MD behaves differently. During the reruns the transmittance decreases whenever the temperature increases, and vice versa. Obviously, these changes of transmittance are due to the remaining MD and not induced by pyrolysis or combustion of carbonaceous compounds. As hematite has already been identified as the light absorbing compound in MD, several filters were loaded with hematite and analyzed as reference samples. To confirm the suitability of hematite as a reference compound, PXRD measurements were performed before and after TOA for a subset of the filters loaded with snow. Hematite was clearly identifiable in all samples. Due to the high background of the filter matrix and the rather low dust loadings a more detailed specification of hematite could not be obtained. The changes in transmittance of Fe_2O_3 during TOA are shown exemplary for a filter loaded with 15 µg Fe cm^{-2} in Figure 1d. Again, replicate analyses (three reruns) were performed. Results of the first run are not shown, as marked differences of the transmittance signal were observed between the first measurement and the reruns, which could be attributed to the evolution of carbonaceous material attached to the hematite (total carbon approx. 5 µgC cm^{-2}). The procedure to omit the first run is in accordance with Wang et al. (2012) and Yamanoi et al. (2009), who also preheated the hematite once before further analyses were conducted. The change in the transmittance signal of hematite compares well to the results of the snow

sample containing MD (Figure 1b), showing an opposing trend of transmittance and temperature. The variation spans an overall range of approximately 500 a.u. and the minimum values are found at highest temperatures. The variation of transmittance which can be attributed exclusively to hematite is lower than the variation usually observed during the first run

160 of analyses, when carbonaceous compounds are present. Still, it is large enough to markedly affect the determination of the split point and explains why the initial value of transmittance cannot be reached at all, when MD loadings are high.
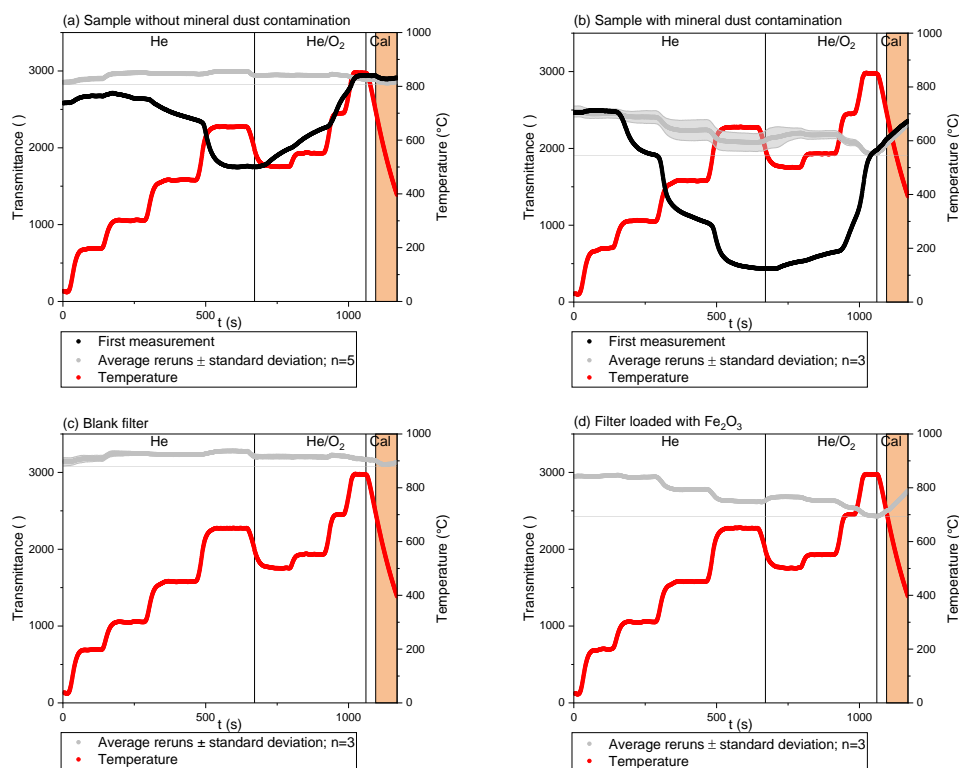
Figure 1: Transmittance during TOA of a snow sample without (a) and with (b) mineral dust contamination, a blank filter (c) and a filter loaded with Fe₂O₃ (d). Details about the filter loadings are given in the text.

During TOA, transmittance is determined at a wavelength of 660 nm where Fe oxide minerals have a rather low absorbing

165 potential compared to shorter wavelength (Alfaro et al., 2004). Therefore, such a severe interference is not expected. However, these evaluations refer to ambient temperature, while high-temperature visible spectroscopy showed that reflectance spectra and colors of hematite changed markedly with increasing temperature up to 800˚C (Yamanoi et al., 2009; Yamanoi and Nakashima, 2005). These changes are especially pronounced at longer wavelength (> 550 nm), meaning that the red color of hematite becomes black with temperature increase (Yamanoi et al., 2009). This phenomenon introduces a severe bias to the

170 determination of the split point, as its position can be expected at a temperature above 500˚C. At that point the darkening of the filter due to MD will be much more pronounced than at the initial temperature or even at the temperature ranges suggested earlier to correct for this bias (Wang et al., 2012; Gul et al., 2018) and a systematic error in the determination of EC occurs. Using the transmittance at 250°C for the determination of the split point, the influence of MD still remains underestimated: At the time of the split point the temperature will definitely be higher and thus the reduction of the transmittance signal due to

175 hematite more pronounced. It would be a mere coincidence if this effect was offset by an early pyrolysis of OC. Using the transmittance at 550°C accounts better for this phenomenon, however, the difference of the black and the grey lines in Figure 1b shows that marked amounts of pyrolytic carbon can be formed at this point of the analysis already, leading to an

overestimation of EC. The error in the determination of EC cannot be quantified based on a single run of analysis and we suggest a second run to assess the relative influences of both, pyrolytic carbon and MD.

180 Replicate measurements of filters with TOA are time consuming. To avoid unnecessary work, the readings of the transmittance signal during the calibration phase can be evaluated. At this point of the analysis all carbon is already removed, a wide temperature range is covered and the gas flow through the main oven maintains oxidizing conditions, like in the second part of TOA when the split point is set. As expected, the transmittance signal is rather constant for the sample without MD contamination (orange part of the graph in Figure 1a) and compares well to the transmittance signal of the blank filter (orange

185 part of the graph in Figure 1c). Samples containing MD show a marked increase in transmittance during the calibration phase, i.e. when the sample is cooling (Figure 1b). The same effect is visible for the reference sample of hematite in Fig. 1d. The change in transmittance during the calibration phase is always visible, during the initial measurement of the sample and for the reruns. Thus, a decision for an additional run of TOA can be based on the calibration phase of the first run. If a marked increase in transmittance is visible, an interference by hematite has to be expected and we recommend to reanalyze the sample.

190 As explained in more detail later, a clear dependence of the transmittance signal on the temperature was observed for samples with hematite loadings above 10 μgFe cm^{-2}.

For completeness we want to mention that high loads of MD might have other influences as well, as precombustion of EC might occur in the presence of inorganic compounds contained in MD, as was shown by Bladt et al., 2012 and Neri et al., 1997.

195 **4.2 Using TOA for Fe$_2$O$_3$ analysis in reference samples**

The evaluation of the transmittance signal logged during the last 75 s of the calibration phase offers more possibilities than a qualitative judgement whether MD might interfere with the OC/EC split point. The sample temperature in this interval changes between slightly above 700°C to slightly below 400°C. To consider the different loadings of the filters, the transmittance data was converted to an attenuation (ATN), defined as ATN = 100 x ln(I_0/I). This conversion follows the approach by Nicolosi et

200 al. (2018), who defined I as the transmittance signal at a particular time step and I_0 as the laser transmittance at the end of the TOA, which reflects an unloaded filter. In our case I refers to a particular temperature rather than to a time step. Furthermore, I_0 is more difficult to determine, as the initial transmittance of the unloaded filter is not reached at the end of the measurement, when the filter remains loaded with hematite. Using the transmittance signal at the end of the calibration phase as reference value I_0', the calculated ATN becomes a relative value, expressing the changes relative to the transmittance at 400°C. This

205 value will always be smaller than the actual ATN of the light absorbing material. Calculating ATN$_{700-400}$ based on the transmittance values at 700°C (I) and 400°C (I_0') we approximate color changes of hematite in this temperature interval. Plotting the hematite loading of the filter expressed as Fe (μg cm^{-2}) versus ATN$_{700-400}$ (Figure 2) shows increasing values of ATN$_{700-400}$ up to hematite loadings of approximately 150 μgFe cm^{-2}. At higher loadings ATN$_{700-400}$ starts to decrease again. This effect is due to the definition of ATN$_{700-400}$ as a relative value, i.e. the difference between the actual ATN at 400°C

210 (ATN$_{400}$) and at 700°C (ATN$_{700}$). ATN$_{400}$ and ATN$_{700}$ relate the transmittance at the respective temperatures to the transmittance value of the unloaded quartz filter at room temperature (I_0). These values could only be approximated, as we did not determine the transmittance values of the unloaded filters. The respective data is presented in the supplement (Fig. S1). As could be expected for filter-based measurements, a linear relationship between hematite loadings and ATN could only be determined for low Fe values, but saturation occurs at higher loadings (Gundel et al., 1984). The onset of this effect is different

215 for ATN$_{400}$ and ATN$_{700}$, i.e. it starts at lower hematite loadings for ATN$_{700}$. Calculating ATN$_{700-400}$ as the difference of ATN$_{700}$ and ATN$_{400}$ leads to the trend shown in Figure 2, and to the unfavorable situation that a defined ATN$_{700-400}$ can be attributed to two hematite loadings. However, this effect is of minor importance for actual analysis, as such high hematite loadings are rarely found.
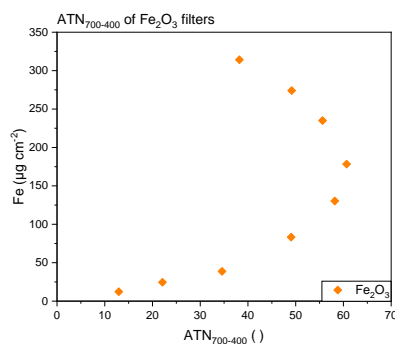
220   **Figure 2: Fe loading of Fe₂O₃ samples determined via ICP-OES plotted versus ATN₇₀₀₋₄₀₀.**

4.3 Applying TOA for the determination of hematite in snow and PM_{10} samples

Applying the approach described above to filters loaded with snow, a similar trend is obtained, although the snow samples generally give smaller values of $ATN_{700-400}$ (Figure 3) compared to the measurements with pure hematite (Fig. 2). We attribute this to differences in the overall loadings of the filters (i.e. the loading with other material than hematite) and the particle sizes.

225   SEM analyses of selected filters confirmed such differences. Hematite particles of the reference material were generally larger in size compared to particulate matter filtrated out of the snow samples. Furthermore, the snow samples showed high loadings of different kinds of particles and just a minor contribution of hematite, which obviously leads to lower ATN values. Examples of the SEM analyses are given in the Supplement (Fig. S2).
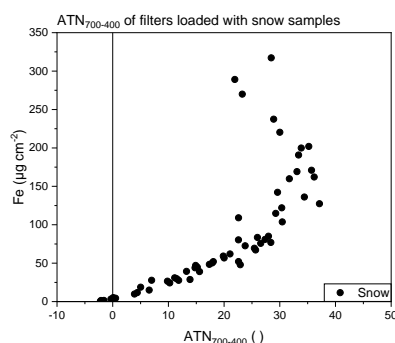
230   **Figure 3: Fe loading of snow samples determined via ICP-OES plotted vs. ATN₇₀₀₋₄₀₀.**

Restrictions have to be set to define a range which allows a definite allocation of $ATN_{700-400}$ to an Fe loading. It is easily possible to distinguish between samples of the upper and lower part of the curve, as Fe loadings above 150 µg cm^{-2} always show transmittance values below 600 a.u. at a temperature of 400°C in the calibration phase. Thinking of actual hematite loadings in filtrated snow samples, Fe loadings above 150 µg cm^{-2} are hardly found. Additionally, an upper and lower limit

235   for $ATN_{700-400}$ values was set. The upper limit (i.e. $ATN_{700-400} < 29$) excludes values with higher variation, while the lower limit (i.e. $ATN_{700-400} > 3.5$) accounts for samples without MD, which do not show a distinct relationship between the transmittance and the sample temperature (see Figure 1). Hence, these samples show very low or even negative values of $ATN_{700-400}$. Based on the mentioned restrictions (transmittance > 600 a.u. at 400°C in the calibration phase and $3.5 < ATN_{700-400} < 29$) Fe loadings reaching from 10 µg cm^{-2} to 100 µg cm^{-2} become accessible via TOA.

240 The selected data points are presented in Fig. 4. A fit was computed applying the least square approach to calculate Fe loadings based on the $ATN_{700-400}$ values. The resulting function is $Fe(\mu g\ cm^{-2})=2.9144*ATN_{700-400}$ and features a coefficient of determination R^2 of 0.9691. The difference between the calculated and the measured Fe loadings divided by the measured Fe loading was below 10% for 20 of 34 samples, above 25% for 7 samples, the maximum being 41% and the median 8%.

To check whether the fit is also applicable for PM_{10} samples, ambient air filters obtained at the Sonnblick Observatory were

245 analyzed and evaluated in the same way. Loadings above 10 µgFe cm⁻² were hardly achieved during the long-term data set, covering June 2017 to March 2021. Only two samples out of a data set showed Fe loadings high enough to be evaluated. They are in good agreement with the model obtained for the snow samples. The samples were collected in January 2020 and February 2021 and represent events with long range transport of desert dust to the high alpine site. These data points are also included in Figure 4 (blue points). Applying the fit calculated for the snow samples, the relative differences between the Fe loadings

250 determined with TOA and with ICP-OES were 6 % and 24 % for these two PM_{10} samples.
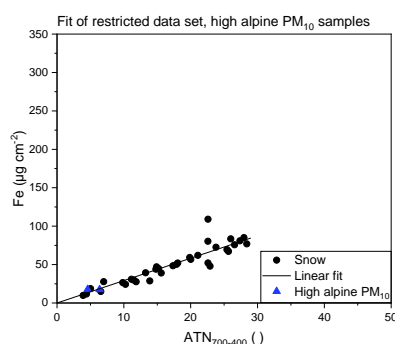
Figure 4: Linear fit for Fe loading and ATN$_{700-400}$ in snow samples and comparison with high alpine PM$_{10}$ samples showing sufficiently high Fe loadings.

For snow samples and PM_{10} samples from a high alpine environment, the evaluation of $ATN_{700-400}$ allows the quantification

255 of Fe between 10 and 100 µg cm⁻² from TOA transmittance data using the same linear approach. Higher Fe loadings can be identified with TOA, but should not be quantified. As the snow samples were collected over a time period of two years, a variety of transport events is included in this evaluation. Still, we want to point out that different source regions might lead to differences in the composition and particle size distribution of MD, which might influence such a fit. Nevertheless, the applicability of the fit to at least a limited number of PM_{10} filters sampled in the same high alpine environment is a promising

260 result.

To test whether the approach is generally applicable for aerosol samples with marked contributions of Fe compounds, we included samples collected within a railway tunnel. This represents a completely different environment as very high Fe contributions and different Fe compounds, like magnetite, hematite and Fe metal, can be expected (Eom et al., 2013). Fe

265 accounts for up to 73% of particulate matter mass, but no specification of Fe compounds has been performed for our samples. All 79 filters evaluated are shown in Figure 5a, together with the other data sets presented within this work. No correlation between $ATN_{700-400}$ and Fe loadings was found for the samples collected in the railway tunnel, although loadings reach up to 325 µgFe cm⁻². The transmittance at 400°C during the calibration phase was never below 600 a.u., which was the case for the samples containing mainly or only hematite at Fe loadings above 150 µg cm⁻². Only 26 samples show an $ATN_{700-400} > 3.5$ and

270 thus meet the criteria for the evaluation based on $ATN_{700-400}$. All other samples featured values for $ATN_{700-400}$ below 3.5, partly even negative values. Even tunnel samples with Fe loadings up to 133 µg cm⁻² showed negative values for $ATN_{700-400}$. All tunnel samples are shown in Figure 5b. "Tunnel PM$_{10}$, Crit" is the subset of samples, which meets the criteria defined for an

unambiguous evaluation of hematite in snow. While snow samples that do not meet the criteria featured Fe loadings either below 10 or above 100 µg cm^{-2}, tunnel samples that do not meet the criteria are found across the whole range of Fe loadings,

275 i.e. 2 to 325 µg cm^{-2}. Despite the high Fe loading on the tunnel filters, automatic split points could be set for most of the tunnel samples. The temperature dependent influence of the Fe loads on the transmittance signal was smaller compared to the changes in transmittance deriving from carbonaceous compounds.

This discrepancy between snow samples and tunnel samples is due to the different origin and form of Fe present and could also be noticed via visual inspection of the filters after TOA, as they were differently colored. Photos of two filters are presented

280 in the Supplement (Fig. S3).

The comparison of all sample groups underlines that the evaluation of ATN$_{700-400}$ is limited to samples containing hematite. If other forms of Fe are expected, the evaluation cannot be applied.
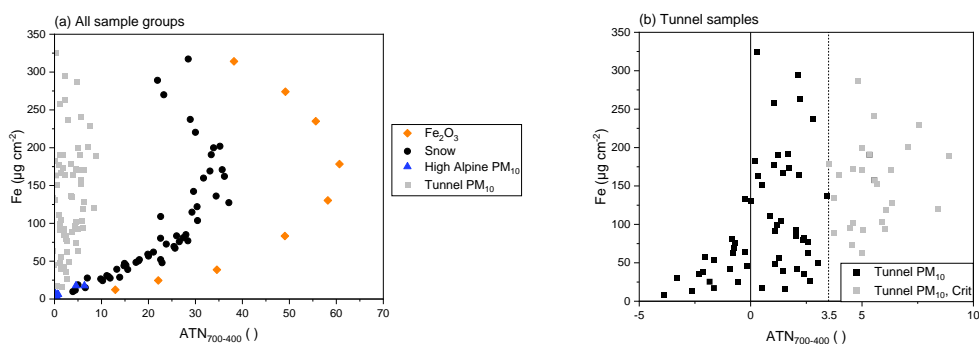
Figure 5: Fe loadings of all sample groups vs. ATN$_{700-400}$ (a) and Fe loading of PM$_{10}$ samples from tunnel measurements vs. ATN$_{700-400}$ (b).

5 Conclusion

285 Based on the detailed evaluation of the temperature induced changes of the transmittance signals obtained during TOA, we presented an easily applicable approach to determine hematite loadings. The method is based on the evaluation of quartz fiber filters either loaded with snow samples containing different amounts of MD or Fe$_2$O$_3$ as a reference compound. All data was obtained using the EUSAAR2 protocol, but only the signals determined during the calibration phase are considered. As this temperature range is also covered by the calibration phase of other commonly used thermal protocols, e.g. IMPROVE_A or

290 NIOSH-like protocols, the evaluations remain valid for these protocols as well. Note that the evaluation was conducted using the transmittance and not reflectance signal. Post-processing of data already available is possible, as no adjustment of the widely used thermal protocols is necessary.

Considering the whole range of Fe loadings investigated, the relationship between the Fe loading and ATN$_{700-400}$ was shown to be non-linear. By setting two straightforward criteria (ATN$_{700-400}$ between 3.5 and 29 and transmittance signal at 400°C

295 above 600 a.u.) the determination of hematite loadings between 10 to 100 µgFe cm^{-2} becomes possible based on a linear approach. Filters loaded that heavily with hematite experience a severe bias of the OC/EC split point. EC will be underestimated or cannot be determined at all.

The work was motivated by two aims. The first one was to better characterize the interference in TOA caused by MD, mainly hematite, and to suggest a method for correction. We recommend to rerun the analyses, as soon as the evaluation of the

300 transmittance signal in the calibration phase indicates an influence of MD. This second run of analyses will allow to set the split point more precisely. Unfortunately, we could not evaluate such a procedure yet, as an independent method for the

determination of EC would be needed to evaluate the improvement. Secondly, the determination of the hematite loading via TOA opens the possibility to obtain another compound of LASI with the same method as used for the determination of EC. This can be advantageous if the available amount of sample is limited.

305 The method developed for the analyses of filters loaded with snow samples was successfully applied to the analyses of particulate matter filters, as long as both types of samples originate from a similar environment. Particulate matter samples collected within a railway tunnel show a different behavior and prove that the method is only suitable for samples that contain Fe in the form of hematite.

Data availability

310 Data can be made available by contacting the corresponding author.

Author Contribution

DK and AKG designed the experiments, performed the data evaluation and interpretation and prepared the manuscript. Analyses were conducted by DK (preparation, TOA and digestion of high alpine and Fe$_2$O$_3$ samples), BK (evaluation of digestion protocols, quality assurance), AG (TOA and digestion of tunnel samples), CH (ICP), EE (SEM) and KH (PXRD).

315 MG performed formal analyses and was responsible for the collection of part of the snow samples. Resources were provided by AKG and AL. All authors contributed to reviewing and editing the manuscript.

Competing interests

The authors declare that they have no conflict of interest.

Acknowledgements

320 Special thanks go to Klaudia Hradil for conducting PXRD-analyses at the X-Ray Center at TU Wien, Austria, and for her valuable input.

References

Alfaro, S. C., Lafon, S., Rajot, J. L., Formenti, P., Gaudichet, A., and Maille, M.: Iron oxides and light absorption by pure desert dust: An experimental study, J. Geophys. Res.-Atmos., 109, D08208, https://doi.org/10.1029/2003JD004374, 2004.

325 Birch, M. E. and Cary, R. A.: Elemental carbon-based method for monitoring occupational exposures to particulate diesel exhaust, Aerosol Sci. Tech., 25, 221-241, https://doi.org/10.1080/02786829608965393, 1996.

Bladt, H., Schmid, J., Kireeva, E. D., Popovicheva, O. B., Perseantseva, N. M., Timofeev, M. A., Heister, K., Uihlein, J., Ivleva, N. P., and Niessner, R.: Impact of Fe content in laboratory-produced soot aerosol on its composition, structure, and thermo-chemical properties, Aerosol Sci. Tech., 46, 1337-1348, https://doi.org/10.1080/02786826.2012.711917, 2012.

330 Bladt, H., Ivleva, N. P., and Niessner, R.: Internally mixed multicomponent soot: Impact of different salts on soot structure and thermo-chemical properties, J. Aerosol Sci., 70, 26-35, https://doi.org/10.1016/j.jaerosci.2013.11.007, 2014.

Cavalli, F., Viana, M., Yttri, K. E., Genberg, J., and Putaud, J. P.: Toward a standardised thermal-optical protocol for measuring atmospheric organic and elemental carbon: the EUSAAR protocol, Atmos. Meas. Tech., 3, 79-89, https://doi.org/10.5194/amt-3-79-2010, 2010.

335   Chow, J. C., Watson, J. G., Pritchett, L. C., Pierson, W. R., Frazier, C. A., and Purcell, R. G.: The DRI thermal/optical reflectance carbon analysis system: description, evaluation and applications in US air quality studies, Atmos. Environ. A.-Gen., 27, 1185-1201, https://doi.org/10.1016/0960-1686(93)90245-T, 1993.

Chow, J. C., Watson, J. G., Chen, L. W. A., Chang, M. O., Robinson, N. F., Trimble, D., and Kohl, S.: The IMPROVE_A temperature protocol for thermal/optical carbon analysis: maintaining consistency with a long-term database, Japca. J. Air

340   Waste Ma., 57, 1014-1023, https://doi.org/10.3155/1047-3289.57.9.1014, 2007.

Degen, T., Sadki, M., Bron, E., König, U., and Nénert, G.: The highscore suite, Powder Diffr., 29, S13-S18, https://doi.org/10.1017/S0885715614000840, 2014.

Di Mauro, B., Fava, F., Ferrero, L., Garzonio, R., Baccolo, G., Delmonte, B., and Colombo, R: Mineral dust impact on snow radiative properties in the European Alps combining ground, UAV, and satellite observations, J Geophys. Res.-Atmos., 120,

345   6080-6097, https://doi.org/10.1002/2015JD023287, 2015.

DIN e.V.: DIN EN 16909:2017, Außenluft - Messung von auf Filtern gesammeltem elementaren Kohlenstoff (EC) und organisch gebundenem Kohlenstoff (OC); Deutsche Fassung EN 16909:2017, Beuth Verlag GmbH, Berlin, 2017.

Doherty, S. J., Hegg, D. A., Johnson, J. E., Quinn, P. K., Schwarz, J. P., Dang, C., and Warren, S. G.: Causes of variability in light absorption by particles in snow at sites in Idaho and Utah, J. Geophys. Res.-Atmos., 121, 4751-4768,

350   https://doi.org/10.1002/2015JD024375, 2018.

Eom, H. J., Jung, H. J., Sobanska, S., Chung, S. G., Son, Y. S., Kim, J. C., Sunwoo, Y., and Ro, C. U.: Iron speciation of airborne subway particles by the combined use of energy dispersive electron probe X-ray microanalysis and Raman microspectrometry, Anal. Chem., 85, 10424-10431, https://doi.org/10.1021/ac402406n, 2013.

Forsström, S., Isaksson, E., Skeie, R. B., Ström, J., Pedersen, C. A., Hudson, S. R., Berntsen, T. K., Lihavainen, H.,

355   Godtliebsen, F., and Gerland, S.: Elemental carbon measurements in European Arctic snow packs, J. Geophys. Res.-Atmos., 118, 13-614, https://doi.org/10.1002/2013JD019886, 2013.

Greilinger, M., Schauer, G., Baumann-Stanzer, K., Skomorowski, P., Schöner, W., and Kasper-Giebl, A.: Contribution of saharan dust to ion deposition loads of high alpine snow packs in Austria (1987–2017), Front. Earth Sci., 6, 126, https://doi.org/10.3389/feart.2018.00126, 2018.

360   Grenfell, T. C., Doherty, S. J., Clarke, A. D., and Warren, S. G.: Light absorption from particulate impurities in snow and ice determined by spectrophotometric analysis of filters, Appl. Optics, 50, 2037-2048, https://doi.org/10.1364/AO.50.002037, 2011.

Gul, C., Puppala, S. P., Kang, S., Adhikary, B., Zhang, Y., Ali, S., Li, Y., and Li, X.: Concentrations and source regions of light-absorbing particles in snow/ice in northern Pakistan and their impact on snow albedo, Atmos. Chem. Phys., 18(7), 4981-

365   5000, https://doi.org/10.5194/acp-18-4981-2018, 2018.

Gundel, L. A., Dod, R. L., Rosen, H., and Novakov, T.: The relationship between optical attenuation and black carbon concentration for ambient and source particles, Sci. Total Environ., 36, 197-202, https://doi.org/10.1016/0048-9697(84)90266-3, 1984.

Kabekkodu, S. N., Faber, J., and Fawcett, T.: New Powder Diffraction File (PDF-4) in relational database format: advantages

370   and data-mining capabilities, Acta Crystallogr. B, 58, 333-337, https://doi.org/10.1107/S0108768102002458, 2002.

Kandler, K., Benker, N., Bundke, U., Cuevas, E., Ebert, M., Knippertz, P., Rodríguez, S., Schütz, L., and Weinbruch, S.: Chemical composition and complex refractive index of Saharan Mineral Dust at Izaña, Tenerife (Spain) derived by electron microscopy, Atmos. Environ., 41, 8058-8074, https://doi.org/10.1016/j.atmosenv.2007.06.047, 2007.

Kang, S., Zhang, Y., Qian, Y., and Wang, H.: A review of black carbon in snow and ice and its impact on the cryosphere,

375   Earth-Sci. Rev., 103346, https://doi.org/10.1016/j.earscirev.2020.103346, 2020.

Karanasiou, A., Diapouli, E., Cavalli, F., Eleftheriadis, K., Viana, M., Alastuey, A., Querol, X., and Reche, C.: On the quantification of atmospheric carbonate carbon by thermal/optical analysis protocols, Atmos. Meas. Tech., 4, 2409-2419, https://doi.org/10.5194/amt-4-2409-2011, 2011.

Kaspari, S., Painter, T. H., Gysel, M., Skiles, S. M., and Schwikowski, M.: Seasonal and elevational variations of black carbon
380   and dust in snow and ice in the Solu-Khumbu, Nepal and estimated radiative forcings, Atmos. Chem. Phys., 14, 8089-8103, https://doi.org/10.5194/acp-14-8089-2014, 2014.

Kuchiki, K., Aoki, T., Niwano, M., Matoba, S., Kodama, Y., and Adachi, K.: Elemental carbon, organic carbon, and dust concentrations in snow measured with thermal optical and gravimetric methods: Variations during the 2007–2013 winters at Sapporo, Japan, J. Geophys. Res.-Atmos., 120, 868-882, https://doi.org/10.1002/2014JD022144, 2015.

385   Li, C., Yan, F., Kang, S., Chen, P., Han, X., Hu, Z., Zhang, G., Hong, Y., Gao, S., Qu, B., Zhu, Z., Li, J., Chen, B., and Sillanpää, M.: Re-evaluating black carbon in the Himalayas and the Tibetan Plateau: concentrations and deposition, Atmos. Chem. Phys., 17, 11899-11912, https://doi.org/10.5194/acp-17-11899-2017, 2017.

Lim, S., Faïn, X., Zanatta, M., Cozic, J., Jaffrezo, J. L., Ginot, P., and Laj, P.: Refractory black carbon mass concentrations in snow and ice: method evaluation and inter-comparison with elemental carbon measurement, Atmos. Meas. Tech., 7, 3307-
390   3324, https://doi.org/10.5194/amt-7-3307-2014, 2014.

Meinander, O., Heikkinen, E., Aurela, M., and Hyvärinen, A.: Sampling, Filtering, and Analysis Protocols to Detect Black Carbon, Organic Carbon, and Total Carbon in Seasonal Surface Snow in an Urban Background and Arctic Finland (> 60° N), Atmosphere-Basel, 11, 923, https://doi.org/10.3390/atmos11090923, 2020.

Neri, G., Bonaccorsi, L., Donato, A., Milone, C., Musolino, M. G., and Visco, A. M.: Catalytic combustion of diesel soot over
395   metal oxide catalysts, Appl. Catal. B-Environ., 11, 217-231, https://doi.org/10.1016/S0926-3373(96)00045-8, 1997.

Nicolosi, E. M. G., Quincey, P., Font, A., and Fuller, G. W.: Light attenuation versus evolved carbon (AVEC)–A new way to look at elemental and organic carbon analysis, Atmos. Environ., 175, 145-153, https://doi.org/10.1016/j.atmosenv.2017.12.011, 2018.

Petzold, A., Ogren, J. A., Fiebig, M., Laj, P., Li, S. M., Baltensperger, U., Holzer-Popp, T., Kinne, S., Pappalardo, G.,
400   Sugimoto, N., Wehrli, C., Wiedensohler, A., and Zhang, X. Y.: Recommendations for reporting" black carbon" measurements, Atmos. Chem. Phys., 13, 8365-8379, https://doi.org/10.5194/acp-13-8365-2013, 2013.

Qian, Y., Yasunari, T. J., Doherty, S. J., Flanner, M. G., Lau, W. K., Ming, J., Wang, H., Wang, M., Warren, S. G., and Zhang, R.: Light-absorbing particles in snow and ice: Measurement and modeling of climatic and hydrological impact, Adv. Atmos. Sci., 32, 64-91, https://doi.org/10.1007/s00376-014-0010-0, 2015.

405   Ramanathan, V. and Carmichael, G.: Global and regional climate changes due to black carbon, Nat. Geosci., 1, 221-227, https://doi.org/10.1038/ngeo156, 2008.

Schwarz, J. P., Gao, R. S., Fahey, D. W., Thomson, D. S., Watts, L. A., Wilson, J. C., Reeves, J. M., Darbeheshti, M., Baumgardner, D. G., Kok, G. L., Chung, S. H., Schulz, M., Hendricks, J., Lauer, A., Kärcher, B., Slowik, K. H., Rosenlof, H., Thompson, T. L., Langford, A. O., Loewenstein, M., and Aikin, K. C.: Single-particle measurements of midlatitude black
410   carbon and light-scattering aerosols from the boundary layer to the lower stratosphere, J. Geophys. Res.-Atmos., 111, D16207, https://doi.org/10.1029/2006JD007076, 2006.

Svensson, J., Ström, J., Kivekäs, N., Dkhar, N. B., Tayal, S., Sharma, V. P., Jutila, A., Backman, J., Virkkula, A., Ruppel, M., Hyvärinen, A., Kontu, A., Hannula, H. R., Leppäranta, M., Hooda, R. K., Korhola, A., Asmi, E., and Lihavainen, H.: Light-absorption of dust and elemental carbon in snow in the Indian Himalayas and the Finnish Arctic, Atmos. Meas. Tech., 11,
415   1403-1416, https://doi.org/10.5194/amt-11-1403-2018 ,2018.

Torres, A., Bond, T. C., Lehmann, C. M., Subramanian, R., and Hadley, O. L.: Measuring organic carbon and black carbon in rainwater: evaluation of methods, Aerosol Sci. Tech., 48, 239-250, https://doi.org/10.1080/02786826.2013.868596, 2014.

Tuzet, F., Dumont, M., Lafaysse, M., Picard, G., Arnaud, L., Voisin, D., Lejeune, Y., Charrois, L., Nabat, P., and Morin, S.: A multilayer physically based snowpack model simulating direct and indirect radiative impacts of light-absorbing impurities in snow, The Cryosphere, 11, 2633-2653, https://doi.org/10.5194/tc-11-2633-2017, 2017.

Tuzet, F., Dumont, M., Picard, G., Lamare, M., Voisin, D., Nabat, P., Lafaysse, M., Larue, F., Revuelto, J., and Arnaud, L.: Quantification of the radiative impact of light-absorbing particles during two contrasted snow seasons at Col du Lautaret (2058 m asl, French Alps), The Cryosphere, 14, 4553-4579, https://doi.org/10.5194/tc-14-4553-2020, 2020.

US EPA: Microwave Assisted Acid Digestion of Siliceous and Organically Based Matrices, OHW, Method 3052, 1996.

Wang, M., Xu, B., Zhao, H., Cao, J., Joswiak, D., Wu, G., and Lin, S.: The influence of dust on quantitative measurements of black carbon in ice and snow when using a thermal optical method. Aerosol Sci. Tech., 46, 60-69, https://doi.org/10.1080/02786826.2011.605815, 2012.

Warren, S. G. and Wiscombe, W. J.: A model for the spectral albedo of snow. II: Snow containing atmospheric aerosols, Journal of Atmospheric Sciences, 37, 2734-2745, https://doi.org/10.1175/1520-0469(1980)037<2734:AMFTSA>2.0.CO;2, 1980.

Yamanoi, Y. and Nakashima, S.: In situ high-temperature visible microspectroscopy for volcanic materials, Appl. Spectrosc., 59, 1415-1419, https://doi.org/10.1366/000370205774783205, 2005.

Yamanoi, Y., Nakashima, S., and Katsura, M.: Temperature dependence of reflectance spectra and color values of hematite by in situ, high-temperature visible micro-spectroscopy, Am. Mineral., 94, 90-97, https://doi.org/10.2138/am.2009.2779, 2009.